Hindawi
Advances in Meteorology
Volume 2020, Article ID 6719160, 15 pages
https://doi.org/10.1155/2020/6719160

Research Article

Ten Years of Aerosol Effects on Single-Layer Overcast Clouds over the US Southern Great Plains and the China Loess Plateau

Hongru Yan and Tianhe Wang

Key Laboratory for Semi-Arid Climate Change of the Ministry of Education, College of Atmospheric Sciences, Lanzhou University, Lanzhou 730000, China

Correspondence should be addressed to Tianhe Wang; wangth@lzu.edu.cn

Received 25 October 2019; Revised 18 January 2020; Accepted 23 January 2020; Published 24 April 2020

Academic Editor: Francisco Molero

Using almost 10 years of observations of clouds and aerosols from the US Southern Great Plains (SGP) atmospheric observatory and the Semi-Arid Climate and Environment Observatory of Lanzhou University (SACOL) in China, the impact of aerosols on single-layer overcast clouds over continental land for different regimes were investigated. Atmospheric conditions at the two sites were first compared in an attempt to isolate the influence of aerosols on cloud properties from dynamic and thermodynamic influences. Cloud types and amounts are similar at the two sites. The dominant aerosol types at the SGP and SACOL sites are sulphate and dust, respectively, with greater aerosol optical depths (AODs) and absorption at the SACOL site. Aerosol first indirect effect (FIE) ranges from 0.021 to 0.152 and from −0.078 to 0.047 at the SGP and SACOL sites, respectively, when using the AOD below cloud base as CCN proxy. Although differences exist, the influence of meteorological conditions on the FIE at the two sites is consistent. FIEs are easily detected under descending motion and dry condition. The FIE at the SGP site is larger than that at the SACOL site, which suggests that the cloud albedo effect is more sensitive under relatively cleaner atmospheric conditions and the dominating aerosol at the SACOL site has less hygroscopicity. The radiative forcing of the FIE over the SGP site is $-3.2\ \mathrm{W\ m^{-2}}$ for each 0.05 increment in FIE. Cloud durations generally prolong as aerosol loading increases, which is consistent with the hypothesis of the aerosol second indirect effect. The negative relationship between cloud duration time and aerosol loading when aerosol loading reaches a large value further might suggest a semidirect effect.

1. Introduction

Since the late nineteenth century, evidences that aerosol particles are essential for forming cloud droplets have been reported by serving as cloud condensation nuclei (CCN) [1–4]. Studies on aerosol-cloud interactions have been conducted for nearly a century and these interactions are still considered to be one of the most important and least known forcings in the climate system [5]. Twomey [6] hypothesized that, under fixed cloud liquid water content conditions, cloud particle sizes decrease with an increasing number of CCN. The reflection of solar radiation off the cloud is then enhanced due to more but smaller cloud droplets in the cloud. This has been referred to as the aerosol first indirect effect (FIE, [7, 8]). A greater number of smaller cloud droplets reduces the precipitation efficiency and increases the cloud liquid water path (LWP), enhancing the cloud lifetime [9]. This phenomenon is referred to as the cloud lifetime effect [7, 9] or the second indirect effect [8]. For deep convective clouds, increasing aerosols might trigger the vertical development of clouds [10–14]. Furthermore, aerosols that strongly absorb solar radiation can generate local heating that, in turn, changes the relative humidity (RH) and the stability of the troposphere and thereby influences cloud formation and lifetime. This is referred to as the semidirect effect [15].

These hypotheses and postulations have been examined using observational, both in situ and satellite, remote sensing data. The magnitudes and even the signs of these aerosol effects are still highly debatable (e.g., [16–19]). The difficulties in quantifying aerosol effects on cloud properties arise for different reasons. First, although aerosol particles

are necessary for cloud droplet formation, dynamic and thermodynamic factors such as RH and vertical motion are also main drivers for cloud formation [20, 21]. Sena et al. [22] found that the impact of macroscopic variables on aerosol-cloud interactions is stronger than the impact of aerosol particles. It is thus hard to fully decouple meteorological influences from aerosol effects. Second, there are some inherent limitations in observation data and/or techniques. Aerosol optical depth (AOD) from clear areas near a cloud has been employed to represent aerosols entering the cloud, as done in many previous studies, but this can incur large uncertainties in relationships between aerosol and cloud properties [23, 24]. Although costly aircraft measurements can solve this problem, using aerosol concentrations near cloud bases is a cost-effective approach with the added benefit of being able to make long-term continuous measurements.

Most previous studies using satellite-based measurements or model simulations (e.g., [19, 25]) have focused on global means. Aerosol-cloud interactions have regional characteristics due to different aerosol properties and meteorological regimes. In situ observations obtained from various short-term intensive field campaigns have been employed in regional studies of aerosol-cloud interactions (e.g., [18, 26]). Huang et al. [27] used satellite-based measurements to compare aerosol-cloud interactions in semiarid regions with similar meteorological environments (in China and USA) and found that, of the two regions, aerosols over China's semiarid region had a larger optical depth, higher absorption, and a more significant semidirect effect [27–31]. A better understanding requires techniques that can combine accurate aerosol and cloud property parameters over an extended period of time to distinguish the impact of aerosols from the natural cloud variability.

Given these uncertainties and difficulties, the goal of this paper is to evaluate and compare aerosol effects on the microphysical, macrophysical, and radiative properties of clouds and to assess their dependence on meteorological conditions by analyzing long-term surface observations made at the US Southern Great Plains (SGP) atmospheric observatory and the Semi-Arid Climate and Environment Observatory of Lanzhou University (SACOL). A brief description of datasets used is presented in Section 2. Section 3 compares background meteorological conditions, aerosol properties, and cloud types at the two sites. Section 4 examines the influences of aerosols on cloud microphysical and macrophysical properties for single-layer overcast clouds with cloud-base height less than 1 km [12] over the two sites and discusses their differences. Section 5 summarizes the findings.

2. Data and Method

The SGP site in north-central Oklahoma is a field measurement site established by the US Department of Energy's Atmospheric Radiation Measurement (ARM) Program. The site is a rural, continental site that experiences a variety of aerosol conditions and cloud types. The other site is the SACOL located on the Loess Plateau in China, a typical semiarid region downwind of desert regions. This site is operated by the Key Laboratory of Semi-Arid Climate Change of the Lanzhou University and is equipped with several advanced instruments. All parameters from these two sites, as well as their uncertainties, the algorithms used to retrieve them, and the measurement periods are outlined in Table 1 and described next.

2.1. Aerosol Properties. The aerosol proxy used for the SACOL and SGP sites is the AOD below the cloud base, which can be calculated by summing up the aerosol extinction coefficient from surface to cloud base. For SACOL, both cloud base height (CBH) and extinction coefficient profile are retrieved from the attenuated backscatter intensity of a micropulse lidar (MPL). Detailed information about cloud height will be given in Section 2.2. The retrieval method of extinction coefficient is according to Fernald method [43] and assuming proper extinction-to-backscatter ratio [33, 44]. To minimize the impacts of water vapor on aerosols, we use the vertical profile from surface to 60 m below the CBH. The MPL can provide continuous day and night measurements at a sampling rate of 60 s. As condensation nuclei concentration number (CN) has a closer relationship with cloud droplets than AOD, CN at the surface measured by a TSI model 3010 condensation particle counter are also employed at the SGP site. However, no same CN measurement is available at the SACOL site. The condensation particle counter works day and night with 60 s sample intervals. When the CBH is constrained to less than 1 km, the CN at the surface can be assumed to be proportional to aerosols injected into a cloud. Thus, clouds at both sites are constrained to base heights less than 1 km. To compare the chemical composition and optical property of aerosols at the two sites, two long-term global datasets, Monitoring Atmospheric Composition and Climate (MACC) reanalysis [34] and Ozone Monitoring Instrument (OMI) [35], are also utilized to give a climatology of aerosol types. Available periods and other information about datasets are summarized in Table 1.

2.2. Cloud Properties. The cloud vertical distribution at the SGP site is obtained from the Active Remote Sensing of CLouds (ARSCL) value-added product, which provides the number of cloud layers (up to a maximum of 10 layers), CBHs, and cloud-top heights (CTHs). This product combines data from a MilliMeter wavelength Cloud Radar (MMCR), ceilometers, and an MPL [36]. At the SACOL site, the number of cloud layers and corresponding CBHs and CTHs are retrieved from MPL measurements [37]. Given that CTH retrievals are only reliable when the signal-to-noise ratio above the cloud top is small, the value of CTH is not used herein. Only single-layer shallow clouds with CBH less than 1 km are chosen in this study.

At both sites, the cloud optical depth (τ) is retrieved from measurements made by an unfiltered silicon pyranometer and a multifilter rotating shadowband radiometer (MFRSR), which is a seven-channel radiometer with six bands of 10 nm full width at half maximum centered near visible and near-

Table 1: Description of data used in the study.

	Parameters	Temporal/ spatial resolutions	Instruments and models	Manufacturer and/or retrieval algorithm	Period
Aerosol	CN concentration	60 sec	CPC	SGP : TSI model 3010	2000.01–2010.03
	Aerosol optical depth single-scattering albedo	60 sec	MPL	SGP : Sigma Space Corporation, [32] SACOL : NASA Goddard Space Flight Center, [33]	2007.03–2015.06
	Aerosol types	3 hours	MACC	[34]	2007.01–2012.12
	Absorbing aerosol index	Daily	OMI (Aqua)	[35]	2004.10–2017.12
Cloud (ground-based)	Cloud top/base height	10 sec 60 sec	MMCR, ceilometer, MPL MPL ()	SGP : MMCR from NOAA environmental research laboratories, [36] SACOL: [37]	2000.01–2010.032007.03–2015.06
	Cloud optical depth	60 sec	MFRSR () MFRSR ()	Both sites: MFRSR from Campbell Scientific, Inc. SGP: [38] SACOL: [39]	2000.01–2010.03 2007.03–2015.06
	Liquid water path				
	Precipitable water	20 sec 60 sec	MWR MWR	Both sites: MWR from radiometrics corporation SGP: [40] SACOL, [27]	2000.01–2010.03 2007.03–2015.06
	Cloud albedo	4 km/30 min	GOES	NB-BB conversion algorithm [41]	2000.01–2010.03
Meteorology	Precipitation	60 sec 60 sec	Rain gauge	SGP : NovaLynx Corp. SACOL : Belfort Instrument Company	2000.01–2010.03 2007.03–2015.06
	Vertical velocity CAPE	1 hour 3 hours	RUC ECMWF	SGP: [6, 7] SACOL: [42]	2000.01–2010.03 2007.03–2015.06

Table 2: Aerosol-mediated shortwave cloud radiative forcing at the SGP site.

LWP (g m^{-2})	20–70	70–120	120–200	200–400	400–600
Forcing (W m^{-2})	−3.99	−6.05	−2.60	−7.55	−10.22

infrared channels. The temporal resolution of the measurements is 20 s and 60 s at the SGP and SACOL sites, respectively. For retrievals of both liquid and ice τ, we take advantage of simultaneous spectral measurements of direct-beam and total radiation from the MFRSR and differences in the ice and liquid cloud particle scattering phase functions [38, 39, 45]. Compared to other surface-based retrieval techniques, this method develops a simple correction scheme that effectively removes radiation scattered in the forward direction by a cloud [46]. t used in this study is based from total radiation rather than direct-beam, which makes it suitable for not very thin cloud. The uncertainty of t is less than 5% [39].

Column-integrated amounts of water vapor and LWP at the SGP and SACOL sites were retrieved from measurements made by a microwave radiometer (MWR). The SGP MWR measures brightness temperatures at two channels (23.8 and 31.4 GHz) and applies a statistical retrieval method developed by [40]. The SACOL MWR (TP/WVP-3000) has 12 channels and uses brightness temperatures at 23.8 and 30 GHz for its retrievals and applies an improved statistical retrieval method [47, 48]. To avoid large retrieval error when LWP is small [49], clouds with LWP less than 20 g m^{-2} are eliminated. In addition, the cloud droplet particle size, or effective radius (r_e), is derived from $(3LWP/2\rho_l\tau)$

[38], where ρ_l is density of liquid water. Errors of r_e are 1.5 and 3 μm for LWP less than 250 g·m^{-2} and greater than 250 g·m^{-2}, respectively.

In short, cloud LWP, τ, r_e, and cloud vertical information over the SGP and SACOL sites are derived from the MWR, the MFRSR, and active remote sensing instruments (MPL and MMCR). In addition, the Geostationary Operational Environmental Satellite (GOES) platform provides cloud albedo information for the SGP site using narrowband-to-broadband conversion formulas [41].

2.3. Meteorology. To examine the thermodynamic effect on aerosol-cloud interactions, daily ERA-Interim reanalysis data [42, 50], a global atmospheric reanalysis produced by the European Centre for Medium-Range Weather Forecasts (ECMWF), was used for the SACOL site. The spatial resolution of the numerical weather prediction system (IFS–CY31r2) used by ERA-Interim is approximately 80 km (T255 spectral). ECMWF interpolated data in regular grid of various spatial resolution ranged from 0.125°*0.125° to 3°*3°. The spatial resolution of the ERA-Interim is ~0.125° and the temporal resolution is three hours. For the SGP site, a North American analysis data with the spatial and temporal resolutions of 20 km and 1 hour from the Rapid Update Cycle (RUC, [51, 52]), which is an operational atmospheric prediction system comprised primarily of a numerical forecast

model and an analysis system to initialize that model, was also used in this study. It has been demonstrated that ECMWF and RUC show good performance in SACOL and SGP sites [53], respectively. Data are interpolated spatially and temporally. Rain gauge data at both sites were also used to remove the rain cases. For studies of climatology at both sites, other long-term auxiliary reanalysis data are utilized.

2.4. Methodology. Ground and space measurements are continuous at both the SACOL and SGP sites with different spatial covering and temporal frequencies. Firstly, based on previous studies [54–56], the optimal match method of different observation is that satellite dataset is averaged over a 20 km × 20 km area around the site and surface observations are averaged over 30 min centered on the satellite overpass time. Then, the study uses several ground-based active instruments to selected out cases meeting with single-layer cloud and CBH less than 1 km. If cases are with raining during the 30 min, corresponding aerosol proxy is used, the 30-min averaged CN, before raining. Finally, aerosol effects on cloud microphysical and macrophysical properties over two sites have been compared and discussed.

3. Climatology of the Two Sites

The geography and climatology at the SGP and SACOL sites have similarities and differences. Both sites are located in the same latitudinal zone (~35°N) and in the inner part of their respective continents. Their altitudes differ; that is, the SGP site is located at 320 m above sea level (ASL) and the SACOL site is located at 1965.8 m ASL. Land surface types at the SGP and SACOL sites are cropland and grassland, respectively. The topography around the SACOL site is characterized by the Loess Plateau consisting of a plain, a ridge, and a mound plain. The terrain where measurements are made is flat and covered with short glass [57].

Studying the similarity and difference in aerosol-cloud interactions in different regions will help us improve the understanding of underlying mechanism. However, differences in meteorology dominate changes in air mass properties, which in turn dominate changes in cloud properties. This makes it difficult to separate aerosol and meteorological effects when studying aerosol-cloud interactions. Before comparing aerosol indirect effects over the two sites, differences in their climatology, cloud coverages, cloud types, aerosol loadings, and aerosol types need to be examined.

3.1. Environmental Conditions. Surface air temperature, RH, and convective available potential energy (CAPE) obtained from the ERA-Interim monthly reanalysis [42, 50] ranging from 1979 to 2015 are used to examine the climatology of the two sites. Precipitation data are from the Global Precipitation Climatology Project (GPCP) Version 2.2 Combined Precipitation Dataset [58], which provides a consistent analysis of global precipitation from an integration of various satellite datasets over land and ocean and a gauge analysis over land.

Figure 1shows the monthly mean surface air temperature, RH, precipitation, and CAPE annual cycles at the two sites. The annual cycles of temperature are similar but the SGP site is generally warmer than the SACOL site by 8 to 11° throughout the year. The annual cycle of RH at the SGP site is almost flat with a small peak in May. The SACOL site is generally 15% drier than the SGP site except in the fall. For both sites, the annual cycles of precipitation and relative humidity have similar trends. More precipitation occurs at the SGP site during the late spring and the early summer and less precipitation occurs during the winter. Precipitation at the SACOL site mainly occurs in summer and early autumn and the amount is 10~90 mm per month less than that experienced at the SGP site. CAPE is associated with vertical motion, which is a key factor in cloud formation. Seasonal trends at both sites are similar to maxima in CAPE in the summer. CAPE at the SGP site is greater than that at the SACOL site. This suggests that the thermodynamic drivers for cloud formation at the SACOL and SGP sites should be different. At the SGP site, the atmosphere should be much more unstable and easily leads to cumulus and convective clouds, which are developed as a consequence of local convection other than advection. It is consistent with the results from a statistical analysis based on five years of CloudSat and Cloud-Aerosol Lidar and Infrared Pathfinder Satellite Observation data [59].

3.2. Cloud Types and Coverage. Almost 30 years of cloud climatology information from the International Satellite Cloud Climatology Project (ISCCP) are used to examine cloud properties at the two sites. The climatology is based on an analysis of measurements of radiances from up to five geostationary and two polar orbiting satellites to infer the global distribution of cloud properties. Depending on cloud-top temperatures, cloud-top pressures, and τ, clouds are classified into nine categories: cumulus, stratocumulus, stratus, altocumulus, altostratus, nimbostratus, cirrus, cirrostratus, and deep convective. ISCCP cloud amounts corresponding to the nine cloud types over the SGP and SACOL sites are shown in Figure 2.

The distributions of cloud amounts for the different cloud types are similar for the two sites. The fractional area covered by low-level clouds is greater at the SGP site; for example, the area covered by stratus clouds at the SGP and SACOL sites is 2.7% and 0.8%, respectively. Concerning mid-level clouds, altocumulus, altostratus, and nimbostratus clouds over the SACOL site cover more area than they do over the SGP site. Concerning high-level clouds, the areal coverage of cirrostratus clouds is greater at the SACOL site than at the SGP site, while the areal coverage of cirrus and deep convective clouds at the SGP site is greater than that at the SACOL site. In this study, warm based shallow clouds are selected. Those clouds include shallow cumulus, stratocumulus, and stratus. Percentages of cumulus, stratocumulus, and/or stratus to total clouds at the two sites were similar.

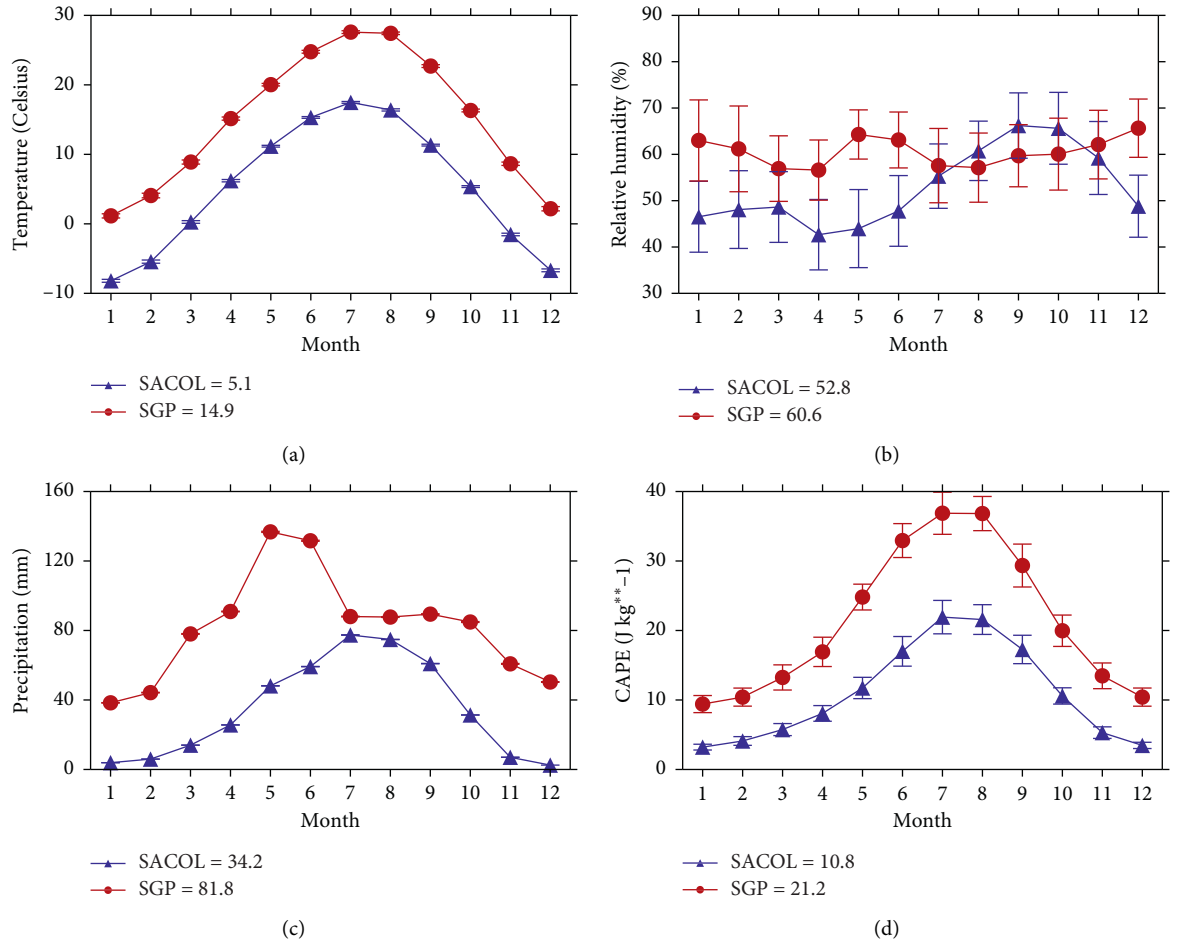

Figure 1: Monthly (a) air temperature, (b) relative humidity from the NCEP reanalysis (1948–2015), (c) precipitation amount from the GPCP (1979–2015), and (d) convective available potential energy (CAPE) from the ECMWF (1979–2015) at the SGP (in red) and SACOL (in blue) sites. Annual mean values are given in the upper left corners of the panels and error bars show the standard deviations.

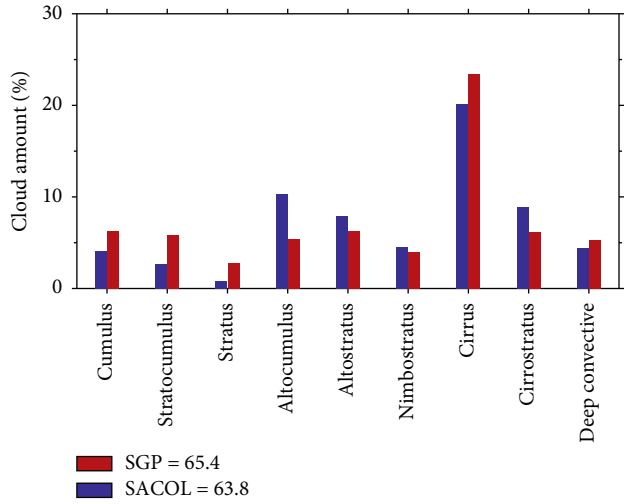

Figure 2: ISCCP cloud amounts for different cloud types at the SGP (red bars) and SACOL (blue bars) sites. Data are from 1980 to 2010. Mean cloud amounts at each site are given in the upper left corner.

3.3. Aerosol Types and Loadings. The eight-year-long reanalysis of atmospheric composition data covering the period of 2003–2010 used here is from the MACC reanalysis, which is provided by assimilating satellite data into the global model and data assimilation system based on the ECMWF's Integrated Forecast System (IFS) [34]. The dataset includes global fields of chemically reactive gases, namely, carbon monoxide, ozone, nitrogen oxides, and formaldehyde, as well as aerosols and greenhouse gases. AODs of sea salt, dust, organic matter, black carbon, and sulphate at the SGP and SACOL sites are shown in Figure 3(a). All five aerosol species are present at both sites with dust dominating at the SACOL site and sulphate dominating at the SGP site. For most of aerosol species, the aerosol loadings at the SACOL site are greater than those at the SGP site. The total AOD at the SACOL site (0.4) is double that at the SGP site (0.2). Dust particles can act as ice nuclei and sulphate is an efficient CCN. This difference may have a large impact on the cloud phase.

More than 10 years (2004–2015) of OMI absorbing aerosol index (AAI) data are also used in this study. AAI is based on the spectral contrast of the reflectances at two UV wavelengths, compared to that of a pure Rayleigh atmosphere. This makes the OMI especially suited for distinguishing between UV-absorbing aerosols, such as desert

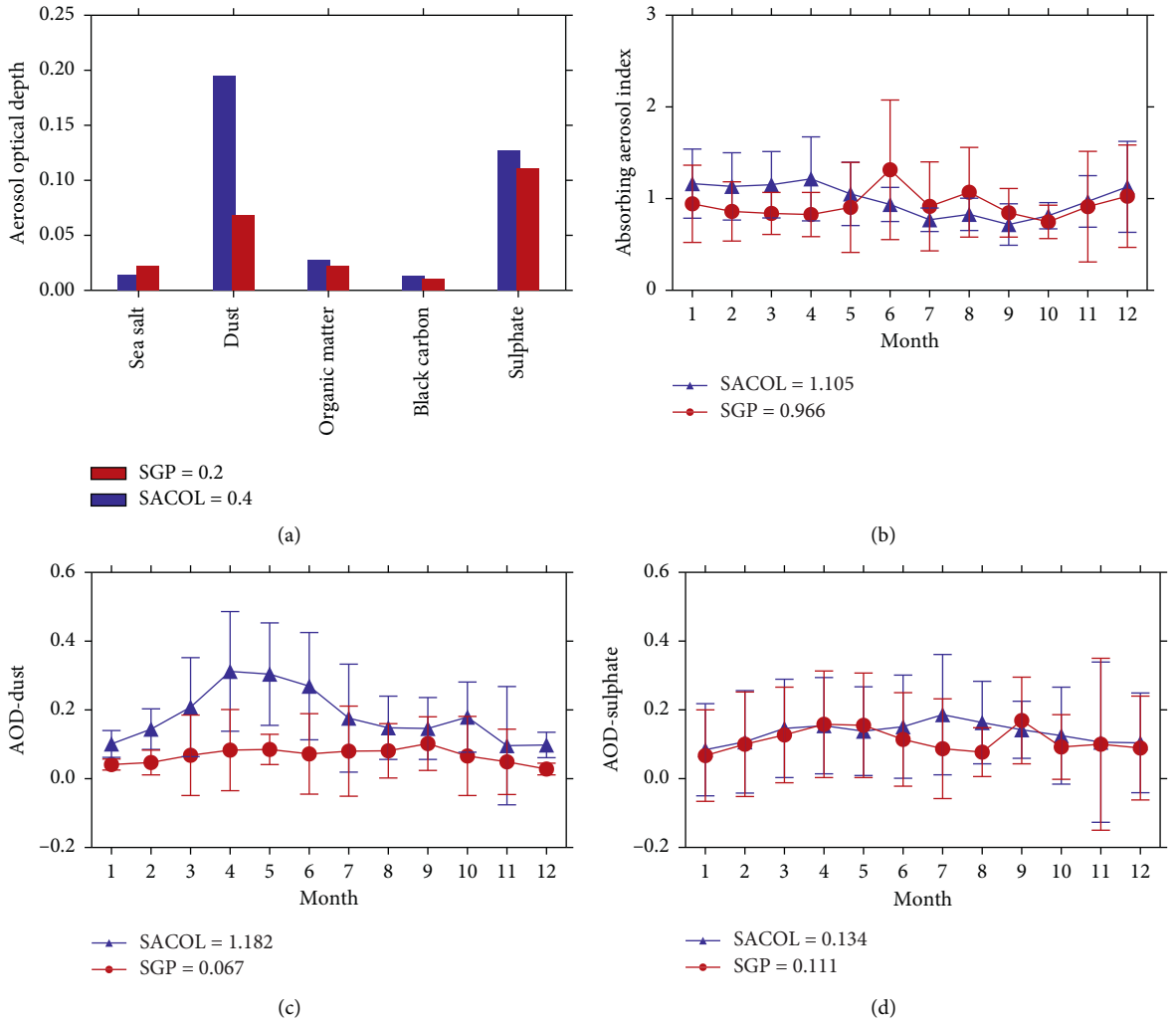

Figure 3: (a) Aerosol optical depth for different aerosol types from the MACC reanalysis (2003–2015) and monthly mean absorbing aerosol index from the OMI (2004–2015) (b), aerosol optical depth of dust (c), and sulphate (d) from MACC at the SGP (in red) and SACOL (in blue) sites. The total AOD at each site is given in the upper right corner of (a). Error bars in (b-d) show the standard deviations.

dust and biomass-burning aerosols, and weakly-absorbing aerosols and clouds. The AAI are near-zero for clouds and weakly-absorbing aerosols and positive for desert dust and biomass-burning aerosols [35]. Annual variations in AAI at the two sites are shown in Figure 3(b). The mean AAI equals 1.105 at the SACOL site, which exceeds that at the SGP site by 14%. This suggests that transported natural dust is the major contributor to the AAI at the SACOL site, which is expected because the site is located near a dust source region having frequent dust events. Huang et al. [60] found that the single-scattering albedo of Taklimakan dust aerosols is about 0.89 at 0.67 μm, which is about 6% less than that of Saharan dust. Ge et al. [61] also obtained the single-scattering albedo about 0.75 at 0.415 μm from MFRSR measurement in East Asian dust event. Logan et al. [62] compared the mineral dust optical properties of two strong Asian dust events from the winter and spring using AERONET-retrieved parameters from the SACOL site and found that there were carbonaceous influences in wintertime and more dust dominating in spring.

4. Results and Discussion

4.1. Aerosol Impact on Cloud Droplet Size. To represent the response of r_e properties to variations in the number of aerosol particles at a constant liquid water content, an FIE index has been proposed by Feingold et al. [63]:

$$\mathrm{FIE} = \left(-\frac{\partial \ln r_e}{\partial \ln \alpha} \right)_{\mathrm{LWP}}, \tag{1}$$

where α is a widely used CCN proxy, such as the aerosol number concentration, AOD, or aerosol light scattering. In this study, AOD below cloud base is used at the SACOL site, and both CN concentration at the surface and AOD below cloud base are used at the SGP site. FIE is defined as positive in sign if an increase in α results in a decrease in r_e. Higher FIE values mean stronger relative changes in cloud microphysics for a relative change in aerosol concentration. This derivative representing the FIE can be used for model validation.

Uncertainties exist in LWP retrievals that limit the attainable accuracy to a certain range of values, which results in an unacceptably large uncertainty for thin clouds [49]. Because of this, cloud cases with LWP less than 20 g·m^{-2} are not considered here. Cases with liquid clouds having CBHs less than 1 km are sorted into several site-specific LWP bins. At the SGP site, the bins are 20–70, 70–120, 120–200, 200–400, and 400–600 g·m^{-2}. At the drier SACOL site, the same bins are applied but the largest bin, 400–600 g·m^{-2}, is not analyzed because of lack of enough samples. Figures 4(a), 4(c), and 4(e) show that LWPs at both sites remain generally constant as the aerosol loading increases, which satisfies the FIE assumption of constant LWP conditions.

Figures 4(b), 4(d), and 4(f) show the relationships between r_e and CN concentration at the SGP site and between r_e and AOD below cloud base at both the SGP and SACOL sites for different LWP bins. No matter using the CN concentration or AOD below cloud base as CCN proxy, r_e decreases as the CN concentration increases in nearly all LWP bins at the SGP site. For clouds with LWP of 70–120 g·m^{-2}, the trend between r_e and CN concentration is inconsistent with the FIE. This may be due to errors in r_e, which is retrieved from τ and LWP in this study. Errors in LWP will lead to errors in r_e. Based on equation (1), values of the FIE at the SGP site in Figure 4(b) are 0.011, −0.010, 0.012, 0.053, and 0.082 for the 20–70, 70–120, 120–200, 200–400, and 400–600 g·m^{-2} LWP bins, respectively. When using the AOD below cloud base as CCN proxy, values of the FIE are, respectively, 0.069, 0.021, 0.05, 0.111, and 0.152 for those LWP bins. These values suggest that the FIE is more pronounced for clouds with large LWP. Values of the FIE at the SACOL site are 0.047, 0.014, −0.078, and −0.025 for the 20–70, 70–120, 120–200, and 200–400 g·m^{-2} LWP bins, respectively. The trends in the 20–70 and 70–120 g·m^{-2} LWP bins reflect the FIE, while no FIE is seen in the other LWP bins. The negative values are caused by meteorological conditions. The reason for negative trends might be increasing cloud droplet collision-coalescence and then increasing r_e with LWP increase. Positive values of the FIE at the SGP site are generally larger than those at the SACOL site.

The phenomenon that increases in FIE as LWP increases at the SGP site is not consistent with that at the SACOL site. For current studies, the dependence of FIE on the LWP over California coast [64], the East China Sea [65], southeast Pacific [66], Nordic Countries [67], and Indian subcontinent [68] showed positive correlations, but it showed negative correlations at Pt. Reyes, California [69], and Azores [20]. Meanwhile, results of no clear dependence of FIE on LWP are also reported by observational study based on both in situ and satellite measurements [70] and a modeling simulation [71]. The reason for negative trends might be increasing cloud drop collision-coalescence and then increasing r_e with LWP increase. For positive trends, aerosol effect on the FIE overwhelms the LWP effect.

Many observational efforts have shown that the FIE can take on a wide range of values (e.g., [72]). Figure 5 compares long-term observed FIE at the SGP and SACOL sites with other current observations of FIE from the literature. Some studies used the cloud droplet number concentration (Nd) instead of r_e. For comparison purpose, all values are converted to the form $(-\partial \ln r_e/\partial \ln \alpha)_{\mathrm{LWP}}$, which is equivalent to $((1/3)(\partial \ln N_d/\partial \ln \alpha))$ [72]. Different CCN proxies, such as aerosol number concentration, aerosol index, AOD, and aerosol scattering coefficient, would also bring discrepancy in FIE values, which were seldom considered in previous works [68, 70, 72]. In Figure 5, different CCN proxies are marked with different symbols. Most of works [20, 25, 26, 64, 65, 67–71, 73–82] use the aerosol number concentration as the proxy, and corresponding values for the FIE range from 0.01 to 0.25. The largest FIE appears over ocean and the smallest FIE over Indian subcontinent. Comparing the FIE with AOD proxy, FIE at the SACOL site is the smallest one and FIE at the SGP site is close to the magnitudes of the global mean FIE. Discrepancy in the magnitudes of the FIE with same aerosol proxy might be due to multiple factors, such as aerosol size, aerosol composition, cloud types, and environmental conditions [20]. Aerosols with low hygroscopicity should have small FIE. Reference [73] also found that the cloud albedo effect is sensitive under relatively clean conditions but is insensitive under polluted conditions. More aerosol loadings and less hygroscopicity of the dominant dust aerosol at the SACOL site might be important reasons why the values of FIE at the SACOL site are smaller than those at the SGP site in Figure 5.

Meteorological factors having the greatest influence on cloud properties, that is, vertical velocity (ω) and precipitable water (PWV) (e.g., [74, 75]) from the ERA-Interim analysis and the MWR, respectively, were used to isolate the indirect effect by comparing the FIE at the SGP and SACOL sites (Figure 6). Data were binned according to ω and PWV. For each grid cell, the FIE in each bin/LWP range was then calculated. In general, the value of FIE decreases as ω increases for all LWP ranges considered. When descending motion ($\omega \leq 0$ m·s^{-1}) dominates, the values of FIE are almost all positive, which suggests that the FIE exists. Under ascending motion conditions, the FIE would go undetected, because the growth of cloud droplets is primarily influenced by adiabatic cooling and collision/condensation rather than by aerosols. Similar trends are observed when the main meteorological component, that is, PWV, was decoupled by restricting the data to several specific PWV ranges. Figure 6(b) shows that the values of FIE are positive and large under dry conditions but negative and smaller under moist conditions. Similar results were reported by [76] that analyzed MODIS products over different regions of the world. Reference [76] found that several effects, such as aerosol swelling [26], partial cloudiness [77], atmospheric dynamics, and cloud three-dimensional [78] and surface influences [79], can lead to this trend.

4.2. Aerosol Impact on Cloud Albedo. Figure 7 shows GOES-retrieved cloud albedo as a function of CN concentration in different LWP bins. For all LWP bins, the cloud albedo increases as the CN concentration increases. For clouds with smaller LWP, cloud albedo changes little as the CN concentration increases. Those trends are generally consistent with the r_e–CN relationship. Note that r_e is derived from MFRSR and MWR ground measurements [38], while the cloud albedo is derived from GOES measurements [41]. Data from different sources supporting each other demonstrates that these trends are robust.

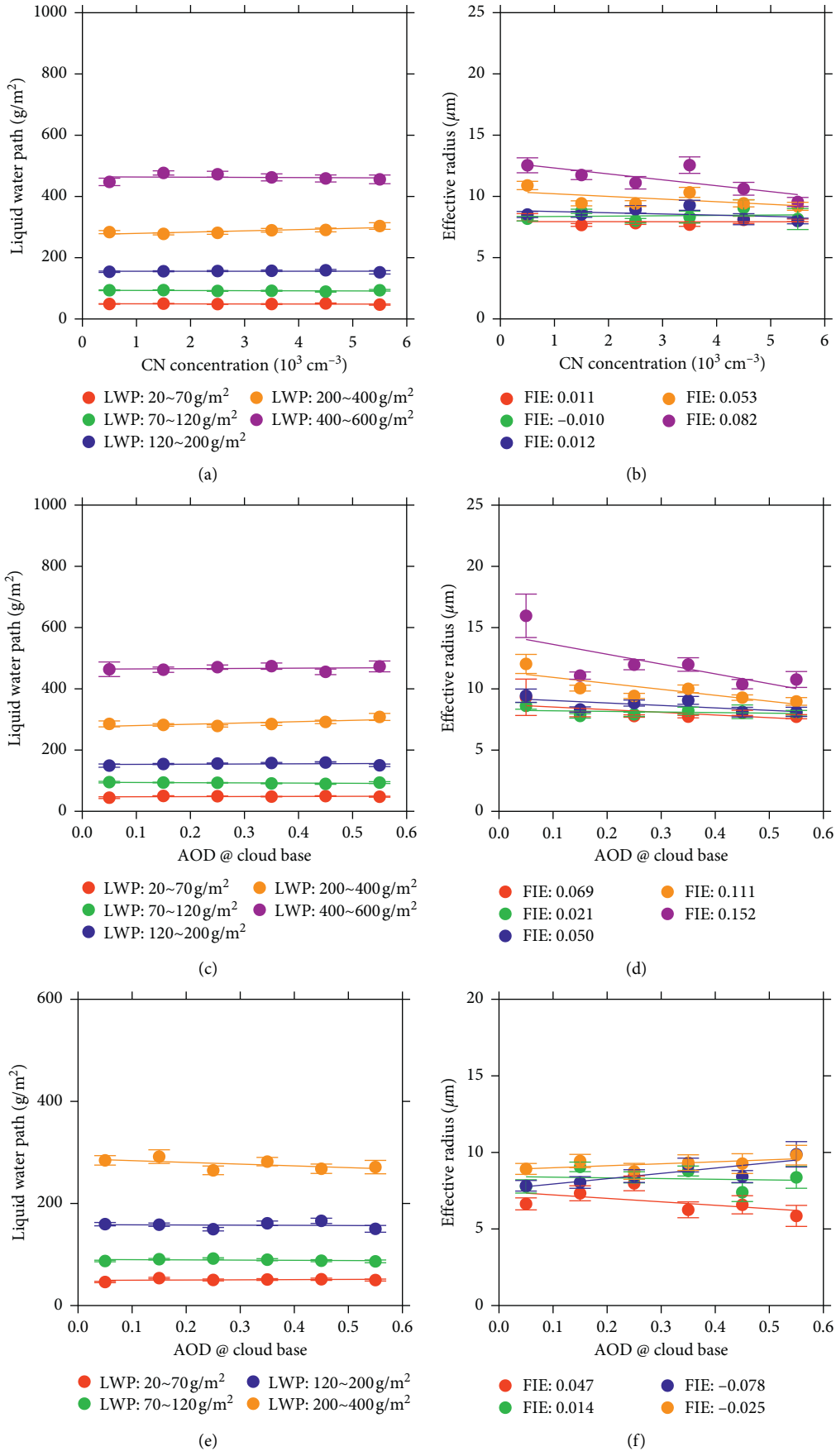

Figure 4: Cloud liquid water path at the (a) and (c) SGP and (e) SACOL sites and cloud effective radius at the (b) and (d) SGP and (f) SACOL sites as a function of aerosol loading for single-layer overcast clouds. Data are binned according to site-specific LWP bins. Values for the aerosol first indirect effect (FIE) are given.

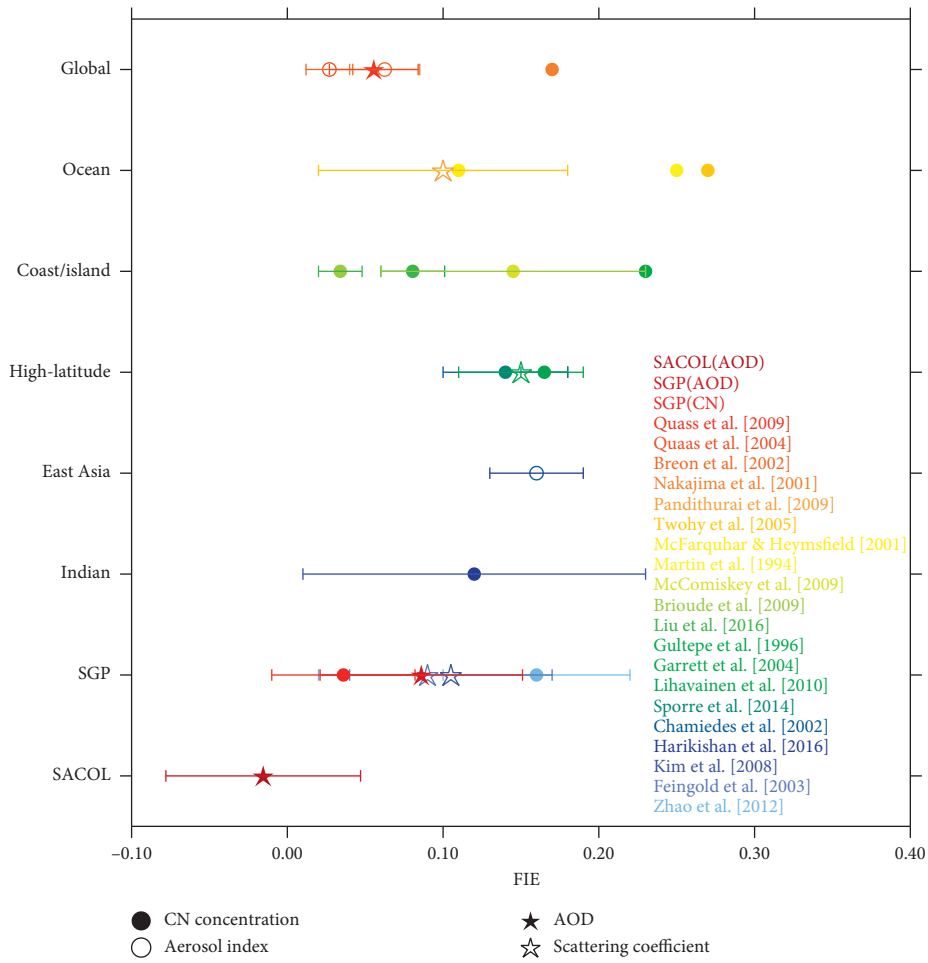

Figure 5: The aerosol first indirect effect (FIE) estimated at the SGP and SACOL sites and from earlier studies. Different CCN proxies used in those studies are sorted out with different symbols.

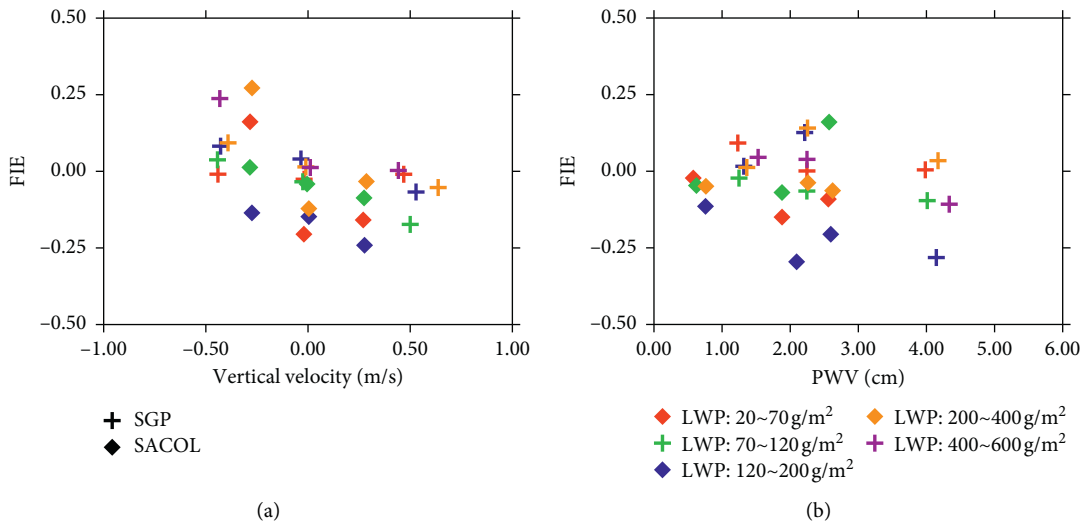

Figure 6: Relationship between the aerosol first indirect effect index, that is, the slope of the linear relationship between cloud droplet effective radius (r_e) and condensation nuclei concentration number (CN), and (a) vertical velocity and (b) precipitable water vapor (PWV) at the SGP (plus signs) and SACOL (squares) sites. Data are binned according to LWP.

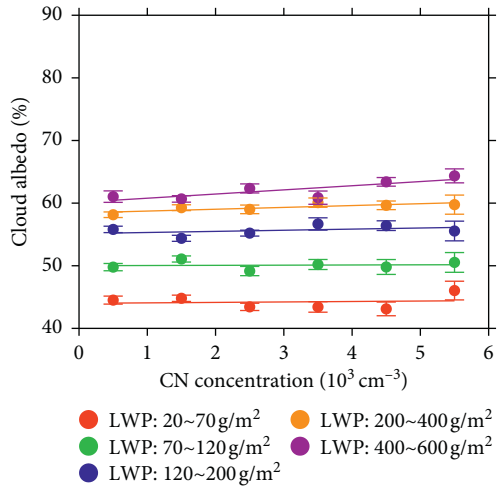

FIGURE 7: Cloud albedo as a function of condensation nuclei concentration number (CN) for shallow warm clouds over the SGP site. Data are binned according to LWP. Error bars show the standard deviations.

The cloud albedo depends on both the cloud droplet size and the cloud optical thickness. These competing effects partially cancel each other making it more difficult to detect an FIE. Based on the relationship between cloud albedo and CN concentration, the shortwave radiative forcing of the FIE can be quantified as follows [14, 80].

First, the relationship between cloud albedo and CN concentration is assumed to be linear, so it is written as

$$\alpha_{\mathrm{cld}}(\mathrm{CN}) = \alpha_{\mathrm{cld}}(\mathrm{CN} = 0) + s * \mathrm{CN}, \quad (2)$$

where α_{cld} is the cloud albedo, s is the slope, and $\alpha_{\mathrm{cld}}(\mathrm{CN} = 0)$ is the y-intercept. The cloud albedo is directly extracted from the GOES product and CN is from ground-based measurements made at the SGP site. The y-intercept and s are calculated using the least-squares approach.

The shortwave radiative forcing induced by the FIE for any aerosol loading can then be calculated as

$$\mathrm{FIE\_RF}(\mathrm{CN}) = S_0 * (\alpha_{\mathrm{cld}}(\mathrm{CN}) - \alpha_{\mathrm{cld}}(CN = 0)), \quad (3)$$

where S_0 is the solar constant (1367 W·m^{-2}). The long-term shortwave radiative forcing from the FIE can be expressed as

$$\mathrm{FIERF} = \mathrm{FIE\_RF}(\mathrm{CN}) * W(\mathrm{CN}), \quad (4)$$

where W (CN) is the weight or frequency of a certain CN concentration. A larger FIERF means that more solar radiation is reflected into space.

FIERF is estimated to be −3.99, −6.05, −2.60, −7.55, and −10.22 W·m^{-2} for LWP bins 20–70, 70–120, 120–200, 200–400, and 400–600 g·m^{-2}, respectively (Table 2). The LWP appears to amplify the cooling effect from the FIE except −2.60 W·m^{-2}, which might result from data sampling uncertainties. Such estimates of FIE derived from measurements may be used to test parameterizations in global-scale models, which has implications for radiative forcing. Quaas et al. [25] evaluated the representation of the FIE in ten different general circulation models (GCMs) using three satellite datasets and found that GCMs tend to overestimate the magnitude of the indirect effect. The global, annual-mean aerosol indirect effect is equal to -0.7 ± 0.5 W·m^{-2}. McComiskey and Feingold [72] quantified the relationship between radiative forcing and changes in FIE over a range of values found in the literature. The difference in radiative flux that occurs as a result of changes in mid-latitude overcast cloud properties for post- versus preindustrial aerosol concentrations ranges from −3 W·m^{-2} to 10 W·m^{-2} for each 0.05 increment in FIE, depending on the anthropogenic perturbation of CCN number ranging from 300 to 2500 cm^{-3} relative to a background value of CCN number equal to 100 cm^{-3}. By applying a linear fit between FIERF and FIE, this difference is −3.2 W m^{-2} for each 0.05 increment in FIE at the SGP site when using CN as CCN proxy. Therefore, an accurate quantification of FIE is needed for better prediction of climate change. Because there are no cloud albedo observations over the SACOL site, FIERF was not calculated for that site.

4.3. Aerosol Impact on Cloud Duration Time. The LWPs of clouds in the real atmosphere change as aerosol loading changes, which is contrary to the assumption underlying the FIE, that is, that the LWP is fixed. The effect of aerosols on clouds without stratification by LWP is a far more complex problem because it involves an evolving system, which includes multiple feedbacks over the life cycle of a cloud. According to GCM estimates, the cloud lifetime effect may be of a similar magnitude with FIE [7].

An increase in aerosol loading will suppress the warm rain process and prolong the lifetime of a cloud, which is a concept that was introduced by modelers but not readily observed in nature. It is impractical to define a cloud lifetime since the existence of a cloud for many hours does not mean that individual parcels of cloudy air exist for many hours. Rather, these parcels cycle in and out of clouds, and cloud elements constantly form and decay. Thus, the cloud duration time is calculated instead of cloud lifetime. Data from instruments that continuously collect observations during the day and night are needed to do this calculation. Radar, lidar, and ceilometer retrievals at the SGP site and lidar retrievals at the SACOL site are used here. Their temporal resolutions are 20 seconds and 60 seconds, respectively. The cloud flag is then processed at a 5-minute temporal resolution. Based on that, the cloud duration can be derived. Only those cases where over 90% of the cloud profiles are single-layer clouds with CBHs less than 1 km and where there is no rain during the cloud duration period are chosen.

Figure 8 shows cloud duration as a function of aerosol loading over the SGP and SACOL sites. Cloud duration times at the SGP site are generally longer than those at the SACOL site. Cloud durations are prolonged as aerosol loading increases at both sites, which is consistent with the aerosol second indirect effect. At the SACOL site, cloud duration times are not monotonically increasing with aerosol loading increases. The trend is positive (negative) when AOD are less (larger) than 0.35. Koren et al. [18] found a similar relationship of cloud amount to AOD over the Amazon and explained it as transition between two

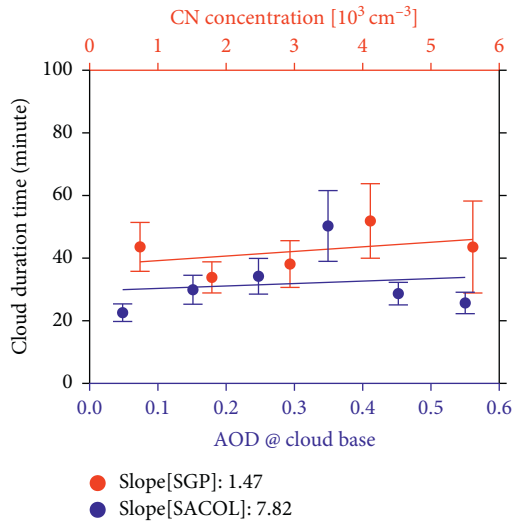

FIGURE 8: Cloud duration as a function of both aerosol CN concentration at the SGP site (red x-axis) and aerosol optical depth below cloud base at the SACOL site (blue x-axis) for shallow warm clouds. Error bars show the standard deviations.

opposing effects of aerosols on clouds: the microphysical and the radiative. Dust aerosol with heavy burden has strong absorption of electromagnetic energy (mostly in the visible and near-infrared range) [60, 61] and then generates local heating that in turn changes the RH and stability of the troposphere and influences cloud formation and lifetime. This is a semidirect effect [15]. Due to lack of the relative location of dust layer to cloud layer, it still cannot exclude other impacts from environment conditions herein. At the SACOL site, [44] compared the saturated layer thickness (thickness of contiguous layers having RH > 85%) in dust and no dust conditions and found that it is more moisture in dust conditions. However, LWP in no dust condition is larger than that in dust condition. The authors therein believed that aerosol increased droplet evaporation due to the semidirect effect. Thus, we can speculate that both the cloud lifetime effect and the semidirect effect involve feedbacks leading to the cloud lifetime change. Using a GCM, Lohmann and Feichter [7] compared the magnitude of all these competing effects and found that the semidirect effect can be important locally, despite the fact that indirect effects dominate globally. Goren and Rosenfeld [81] developed a method for partitioning the components of the aerosol-cloud interaction radiative effect (CRE) of marine stratocumulus into Twomey, cloud cover, and liquid water path effects and examined 50 cases. They showed that, of the three effects, the Twomey effect contributes to only a quarter of the difference in the CRE.

Wind speed around a cloud layer may play a role in the duration time of the cloud. Higher wind speed means faster movement of cloud overhead, as well as shorter cloud duration observed by radar and lidar. Wind speed is the major reason why the cloud duration is distinguished from cloud lifetime. To minimize the influence from wind speed, cloud duration as a function of aerosol loading for different wind speed ranges is shown in Figure 9. As expected, the cloud

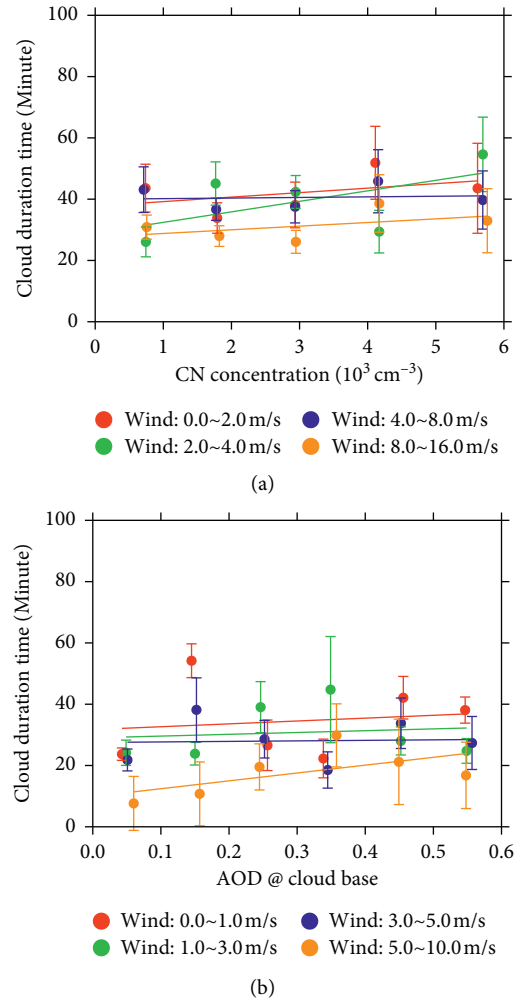

FIGURE 9: Cloud duration as a function of aerosol loading for different wind speed ranges at the (a) SGP and (b) SACOL sites for single-layer clouds. Error bars show the standard deviations.

duration is generally longer under light wind conditions than under stronger ones in our statistical analysis. For all wind speeds, the cloud duration time increases as the aerosol loading increases. It means that the approach to produce cloud duration is rational and cloud duration can denote cloud lifetime if time series used in analysis are long enough.

Anecdotal evidence of clouds in a very clean atmosphere precipitating almost as soon as they form has been noted, but no systematic observations of aerosol effects on cloud lifetime have been reported. A modeling study by [17] showed suppressed precipitation but no effect of aerosol perturbations on the lifetime of populations of cumulus clouds. There is also a suggestion that aerosol effects may depend on the size of the perturbed clouds and that small clouds may respond differently than large clouds.

5. Conclusions

The aerosol indirect effect is still a major source of uncertainty in the simulation of climate changes [5]. Some aspects of linkages between aerosols, clouds, and climate have been

qualitatively confirmed, but there is still considerable debate over their magnitude. Furthermore, the effects of aerosols on cloud fraction, cloud LWP, and cloud lifetime are highly uncertain in sign. This study examined differences in aerosol-cloud interactions between two inland continental sites located in the same latitudinal zone, i.e., the US SGP and China Loess Plateau SACOL sites. We analyzed about ten years of data from both sites in an attempt to isolate the influence of aerosols on cloud properties from dynamic and thermodynamic influences.

Two sites have similar cloud types and corresponding cloud amounts. Sulphate and dust aerosols dominate at the SGP and SACOL sites, respectively, and the total AOD and absorption at the SACOL site are larger than those at the SGP site. At the SGP site, the aerosol FIE, i.e., r_e decreases as the aerosol loading increases, does exist in nearly all LWP bins, while it only exists when cloud LWP ranges from 20 to 120 $g \cdot m^{-2}$ at the SACOL site. FIE at the SGP site ranges from −0.010 to 0.082 (0.021 to 0.152) when using the CN (AOD below cloud base) as CCN proxy. Values of the FIE at the SACOL site range from -0.078 to 0.047. Although the trends in r_e as a function of aerosol loading over the two sites show differences, the influence of ω and PWV on the trends is consistent. FIEs are easily detected under descending motion and dry condition.

The FIE at the SGP site is generally larger than at the SACOL site. A possible explanation for this finding is that the cloud albedo effect is more sensitive under relatively clean conditions. The dust aerosol at the SACOL site with less hygroscopicity might be another important reason. The radiative forcing of the aerosol indirect effect over the SGP site is -3.2 $W \cdot m^{-2}$ for each 0.05 increment in the FIE. The findings presented here have important implications for estimates of aerosol effects on climate forcing.

At both sites, the cloud duration increases as the aerosol loading increases, which is consistent with the hypothesis of the aerosol second indirect effect. The relationship between cloud duration and aerosol loading further might suggest cancelling of the competing influences by cloud lifetime effect and by the semidirect effect. This finding is different from those reported in previous studies, in which the cloud lifetime is hard to derive based on observations. Our approach is based on continuous day and night cloud measurements to produce a cloud duration dataset. Differences in aerosol type and cloud type could definitely make differences in aerosol-cloud interactions; this is just an initial work to reveal the impact of aerosol type on cloud properties. High temporal and spatial resolution dataset about aerosol species and cloud types are needed in the future. Results from this study are physically sound in general, and the quantified estimates of radiative forcing may be useful for evaluating modeling results.

Data Availability

The aerosol and cloud properties datasets of SACOL site are provided by Key Laboratory for Semi-Arid Climate Change of the Ministry of Education, Lanzhou University (http://climate.lzu.edu.cn). All of data referring to SGP site are available from the Atmospheric Radiation Measurement (ARM), a US Department of Energy (DOE) Office of Science user facility (https://www.arm.gov/data). The ERA-Interim dataset is obtained from https://www.ecmwf.int/en/forecasts/datasets/reanalysis-datasets/era-interim. Global Precipitation Climatology Project (GPCP) Version 2.2 Combined Precipitation Dataset is obtained from https://www.esrl.noaa.gov/psd/data/gridded/data.gpcp.html. The cloud climatology is provided by International Satellite Cloud Climatology Project (ISCCP) (https://eosweb.larc.nasa.gov/project/isccp/isccp_d2_table). The Monitoring Atmospheric Composition and Climate (MACC) reanalysis is obtained from https://apps.ecmwf.int/datasets/data/macc-reanalysis/levtype = sfc/.

Conflicts of Interest

The authors declare that they have no conflicts of interest.

Acknowledgments

This work was supported by the Ministry of Science and Technology of China (2017YFC1501403) and the National Natural Science Foundation of China under Grant nos. 41405125 and 41775022. It is also supported by the Foundation of Key Laboratory for Semi-Arid Climate Change of the Ministry of Education in Lanzhou University. The authors are grateful to Beidou Zhang and Tian Zhou from Lanzhou University for their efforts in providing ground-based observations. The authors would also like to thank Zhanqing Li, Jianjun Liu, and Maureen Cribb from University of Maryland, College Park, for their discussions regarding this study.

References

[1] J. Nelkin, "On dust, fogs, and clouds," *Proceedings of the Royal Society of Edinburgh*, vol. 9, no. 14–18, 1880.

[2] P. J. Coulier, "Note sur une nouvelle propriété de l'aire," *Journal de Pharmacie Et de Chimie*, vol. 4, no. 1, pp. 165–172, 1875.

[3] H. Köhler, "The nucleus in and the growth of hygroscopic droplets," *Transactions of the Faraday Society*, vol. 32, pp. 1152–1161, 1936.

[4] C. T. R. Wilson, "Condensation of water vapour in the presence of dust-free air and other gases," *Philosophical Transactions of the Royal Society*, vol. A189, pp. 265–307, 1897.

[5] IPCC, "Climate Change 2013," in *The Physical Science Basis. Contribution of Working Group I to the Fifth Assessment Report of the Intergovernmental Panel on Climate Change*, T. F. Stocker, D. Qin, G.-K. Plattner et al., Eds., p. 1535, Cambridge University Press, Cambridge, UK, 2013.

[6] S. Twomey, "The influence of pollution on the shortwave albedo of clouds," *Journal of the Atmospheric Sciences*, vol. 34, no. 7, pp. 1149–1152, 1977.

[7] U. Lohmann and J. Feichter, "Global indirect aerosol effects: a review," *Atmospheric Chemistry and Physics*, vol. 5, no. 3, pp. 715–737, 2005.

[8] V. Ramaswamy, O. Boucher, J. Haigh et al., "Radiative forcing of climate change," in *Climate Change 2001: The Scientific Basis. Contribution of Working Group I to the Third*

Assessment Report of the Intergovernmental Panel on Climate Change, J. T. Houghton, Y. Ding, D. J. Griggs et al., Eds., pp. 349–416, Cambridge University Press, Cambridge, UK, 2001.

[9] B. A. Albrecht, "Aerosols, cloud microphysics, and fractional cloudiness," *Science*, vol. 245, no. 4923, pp. 1227–1230, 1989.

[10] M. O. Andreae, D. Rosenfeld, P. Artaxo et al., "Smoking rain clouds over the Amazon," *Science*, vol. 303, no. 5662, pp. 1337–1342, 2004.

[11] I. Koren, Y. J. Kaufman, D. Rosenfeld, and L. A. Remer, "Aerosol invigoration and restructuring of Atlantic convective clouds," *Geophysical Research Letters*, vol. 32, no. 14, pp. 4–7, 2005.

[12] Z. Li, F. Niu, J. Fan, Y. Liu, D. Rosenfeld, and Y. Ding, "Long-term impacts of aerosols on the vertical development of clouds and precipitation," *Nature Geoscience*, vol. 4, no. 12, pp. 888–894, 2011.

[13] D. Rosenfeld, U. Lohmann, G. B. Raga et al., "Flood or drought: how do aerosols affect precipitation?" *Science*, vol. 321, no. 5894, pp. 1309–1313, 2008.

[14] H. Yan, Z. Li, J. Huang, M. Cribb, and J. Liu, "Long-term aerosol-mediated changes in cloud radiative forcing of deep clouds at the top and bottom of the atmosphere over the Southern Great Plains," *Atmospheric Chemistry and Physics*, vol. 14, no. 14, pp. 7113–7124, 2014.

[15] J. Isaac, M. Sato, and R. Ruedy, "Radiative forcing and climate response," *Journal of Geophysical Research: Atmospheres*, vol. 102, no. D6, pp. 6831–6864, 1997.

[16] H. Jiang and G. Feingold, "Effect of aerosol on warm convective clouds: aerosol-cloud-surface flux feedbacks in a new coupled large eddy model," *Journal of Geophysical Research*, vol. 111, no. D1, p. D01202, 2006.

[17] H. Jiang, H. Xue, A. Teller, G. Feingold, and Z. Levin, "Aerosol effects on the lifetime of shallow cumulus," *Geophysical Research Letters*, vol. 33, no. 14, p. L14806, 2006.

[18] I. Koren, J. V. Martins, L. A. Remer, and H. Afargan, "Smoke invigoration versus inhibition of clouds over the Amazon," *Science*, vol. 321, no. 5891, pp. 946–949, 2008.

[19] J. E. Penner, L. Xu, and M. Wang, "Satellite methods underestimate indirect climate forcing by aerosols," *Proceedings of the National Academy of Sciences*, vol. 108, no. 33, p. 13404, 2011.

[20] J. Liu, Z. Li, and M. Cribb, "Response of marine boundary layer cloud properties to aerosol perturbations associated with meteorological conditions from the 19-month AMF-azores campaign," *Journal of the Atmospheric Sciences*, vol. 73, no. 11, pp. 4253–4268, 2016.

[21] J. Schmidt, A. Ansmann, J. Bühl, and U. Wandinger, "Strong aerosol-cloud interaction in altocumulus during updraft periods: lidar observations over central Europe," *Atmospheric Chemistry and Physics*, vol. 15, no. 18, pp. 10687–10700, 2015.

[22] E. T. Sena, A. McComiskey, and G. Feingold, "A long-term study of aerosol-cloud interactions and their radiative effect at the Southern Great Plains using ground-based measurements," *Atmospheric Chemistry and Physics*, vol. 16, no. 17, pp. 11301–11318, 2016.

[23] M. O. Andreae, "Correlation between cloud condensation nuclei concentration and aerosol optical thickness in remote and polluted regions," *Atmospheric Chemistry and Physics*, vol. 9, no. 2, pp. 543–556, 2009.

[24] J. Liu and Z. Li, "Estimation of cloud condensation nuclei concentration from aerosol optical quantities: influential factors and uncertainties," *Atmospheric Chemistry and Physics*, vol. 14, no. 1, pp. 471–483, 2014.

[25] J. Quaas, Y. Ming, S. Menon et al., "Aerosol indirect effects - general circulation model intercomparison and evaluation with satellite data," *Atmospheric Chemistry and Physics*, vol. 9, no. 22, pp. 8697–8717, 2009.

[26] G. Feingold, W. L. Eberhard, D. E. Veron, and M. Previdi, "First measurements of the Twomey indirect effect using ground-based remote sensors," *Geophysical Research Letters*, vol. 30, no. 6, p. 1287, 2003.

[27] J. Huang, P. Minnis, H. Yan et al., "Dust aerosol effect on semi-arid climate over Northwest China detected from A-Train satellite measurements," *Atmospheric Chemistry and Physics*, vol. 10, no. 14, pp. 6863–6872, 2010a.

[28] J. Huang, "possible influences of Asian dust aerosols on cloud properties and radiative forcing observed from MODIS and CERES," *Geophysical Research Letters*, vol. 30, p. L06824, 2006a.

[29] J. Huang, "satellite-based assessment of possible dust aerosols semi-direct effect on cloud water path over East Asia," *Geophysical Research Letters*, vol. 33L19802 pages, 2006b.

[30] J. Huang, M. Ji, Y. Xie, S. Wang, Y. Wang, and J. Ran, "Gobal semi-arid climate change over last 60 years," *Climate Dynamics*, vol. 46, no. 3-4, pp. 1131–1150, 2016.

[31] J. Huang, Y. Li, C. Fu et al., "Dryland climate change: recent progress and challenges," *Reviews of Geophysics*, vol. 55, no. 3, pp. 719–778, 2017.

[32] C. Sivaraman, J. Comstock, K. Johnson, C. Flynn, Z. Wang, and S. McFarlane., "Routine cloud-boundary algorithm development for ARM micropulse lidar," in *Proceedings of the Presented at 2nd Atmospheric System Research (ASR) Science Team Meeting*, San Antonio, TX, 2011.

[33] J. P. Huang, Z. W. Huang, J. R. Bi et al., "Micro-pulse lidar measurements of aerosol vertical structure over the Loess Plateau," *Atmospheric and Oceanic Science Letters*, vol. 1, pp. 8–11, 2008.

[34] A. Inness, F. Baier, A. Benedetti et al., "The MACC reanalysis: an 8 yr data set of atmospheric composition," *Atmospheric Chemistry and Physics*, vol. 13, no. 8, pp. 4073–4109, 2013.

[35] O. Torres, A. Tanskanen, B. Veihelmann et al., "Aerosols and surface UV products from OMI observations: an overview," *Journal of Geophysical Research: Atmospheres*, vol. 112, 2007.

[36] E. E. Clothiaux, T. P. Ackerman, G. G. Mace et al., "Objective determination of cloud heights and radar reflectivities using a combination of active remote sensors at the ARM CART sites," *Journal of Applied Meteorology*, vol. 39, no. 5, pp. 645–665, 2000.

[37] H. Xie, T. Zhou, Q. Fu et al., "Automated detection of cloud and aerosol features with sacol micro-pulse lidar in northwest China," *Optics Express*, vol. 25, 2017.

[38] Q. Min and L. C. Harrison, "Cloud properties derived from surface MFRSR measurements and comparison with GOES results at the ARM SGP site," *Geophysical Research Letters*, vol. 23, no. 13, pp. 1641–1644, 1996.

[39] T. Wang and Q. Min, "Retrieving optical depths of optically thin and mixed-phase clouds from MFRSR measurements," *Journal of Geophysical Research: Atmospheres*, vol. 113D19203 pages, 2008.

[40] J. C. Liljegren, "Automatic self-calibration of ARM microwave radiometers," in *Microwave Radiometry and Remote Sensing of the Earth's Surface and Atmosphere*, P. Pampaloni and S. Paloscia, Eds., pp. 433–443, CRC, Horsham Township, PA, USA, 1999.

[41] P. Minnis, W. L. Smith Jr., D. P. Garber, J. K. Ayers, and D. R. Doelling, "Cloud properties derived from GOES-7 for spring 1984 ARM intensive observing period using version

1.0.0 of ARM satellite data analysis program," *NASA RP*, vol. 1366, p. 58, 1995.

[42] P. Berrisford, D. P. Dee, K. Fielding et al., *The ERA-Interim Archive'. ERA Report Series, No.1*, ECMWF, Reading, TX, UK, 2009.

[43] F. G. Fernald, "Analysis of atmospheric lidar observations: some comments," *Applied Optics*, vol. 23, no. 5, pp. 652-653, 1984.

[44] K. Huang, G. Zhuang, J. Li et al., "Mixing of Asian dust with pollution aerosol and the transformation of aerosol components during the dust storm over China in spring 2007," *Journal of Geophysical Research*, vol. 115, p. D00K15, 2010.

[45] Q. Min, E. Joseph, and M. Duan, "Retrievals of thin cloud optical depth from a multifilter rotating shadowband radiometer," *Journal of Geophysical Research*, vol. 109, no. D2, p. D02201, 2004.

[46] E. Joseph and Q. Min, "Assessment of multiple scattering and horizontal inhomogeneity in IR radiative transfer calculations of observed thin cirrus clouds," *Journal of Geophysical Research*, vol. 108, no. D13, p. 4380, 2003.

[47] J. Huang, M. He, H. Yan, B. Zhang, J. Bi, and Q. Jin, "A study of liquid water path and precipitable water vapor in Lanzhou area using ground-based microwave radiometer," *Chinese Journal of Atmospheric Sciences*, vol. 34, no. 548–558, (in Chinese), 2010b.

[48] J. C. Liljegren, E. E. Clothiaux, G. G. Mace, S. Kato, and X. Dong, "A new retrieval for cloud liquid water path using a ground-based microwave radiometer and measurements of cloud temperature," *Journal of Geophysical Research: Atmospheres*, vol. 106, no. 14, 485 pages, 2001.

[49] D. D. Turner, A. M. Vogelmann, R. T. Austin et al., "Thin liquid water clouds: their importance and our challenge," *Bulletin of the American Meteorological Society*, vol. 88, no. 2, pp. 177–190, 2007.

[50] D. P. Dee, "Co-authors: the ERA-Interim reanalysis: configuration and performance of the data assimilation system," *Quarterly Journal of the Royal Meteorological Society*, vol. 137, pp. 553–597, 2011.

[51] S. G. Benjamin, G. A. Grell, J. M. Brown, T. G. Smirnova, and R. Bleck, "Mesoscale weather prediction with the RUC hybrid isentropic/terrain-following coordinate model," *Monthly Weather Review*, vol. 132, pp. 474–494, 2004a.

[52] S. G. Benjamin, D. Dévényi, S. S. Weygandt et al., "An hourly assimilation-forecast cycle: the RUC," *Monthly Weather Review*, vol. 132, no. 2, pp. 495–518, 2004b.

[53] P. Minnis, Y. Yi, J. Huang, and K. Ayers, "Relationships between radiosonde and RUC-2 meteorological conditions and cloud occurrence determined from ARM data," *Journal of Geophysical Research*, vol. 110, no. D23, p. D23204, 2005.

[54] X. Dong, G. G. Mace, P. Minnis et al., "Comparison of stratus cloud properties deduced from surface, GOES, and aircraft data during the march 2000 ARM cloud IOP," *Journal of the Atmospheric Sciences*, vol. 59, no. 23, pp. 3265–3284, 2002.

[55] H. Yan, J. Huang, P. Minnis, T. Wang, and J. Bi, "Comparison of CERES surface radiation fluxes with surface observations over Loess Plateau," *Remote Sensing of Environment*, vol. 115, no. 6, pp. 1489–1500, 2011.

[56] H. Yan, J. Huang, P. Minnis et al., "Comparison of CERES-MODIS cloud microphysical properties with surface observations over Loess Plateau," *Journal of Quantitative Spectroscopy and Radiative Transfer*, vol. 153, no. -, pp. 65–76, 2015.

[57] X. Li, J. Huang, R. Zhang et al., "Surface measurements of aerosol properties over northwest China during ARM China 2008 deployment," *Journal of Geophysical Research*, vol. 115, p. D00K17, 2010.

[58] R. F. Adler, G. J. Huffman, A. Chang et al., "The version-2 global precipitation climatology project (GPCP) monthly precipitation analysis (1979-present)," *Journal of Hydrometeorology*, vol. 4, no. 6, pp. 1147–1167, 2003.

[59] J. Li, J. Huang, K. Stamnes, T. Wang, Q. Lv, and H. Jin, "A global survey of cloud overlap based on CALIPSO and CloudSat measurements," *Atmospheric Chemistry and Physics*, vol. 15, no. 1, pp. 519–536, 2015.

[60] J. Huang, Q. Fu, J. Su et al., "Taklimakan dust aerosol radiative heating derived from CALIPSO observations using the Fu-Liou radiation model with CERES constraints," *Atmospheric Chemistry and Physics*, vol. 9, no. 12, pp. 4011–4021, 2009.

[61] J. M. Ge, J. Su, T. P. Ackerman, Q. Fu, J. P. Huang, and J. S. Shi, "Dust aerosol optical properties retrieval and radiative forcing over northwestern China during the 2008 China-U.S. joint field experiment," *Journal of Geophysical Research*, vol. 115, p. D00K12, 2010.

[62] T. Logan, B. Xi, and X. Dong, "A comparison of the mineral dust absorptive properties between two Asian dust events," *Atmosphere*, vol. 4, no. 1, pp. 1–16, 2013.

[63] G. Feingold, L. A. Remer, J. Ramaprasad, and Y. J. Kaufman, "Analysis of smoke impact on clouds in Brazilian biomass burning regions: an extension of Twomey's approach," *Journal of Geophysical Research: Atmospheres*, vol. 106, no. D19, 2001.

[64] J. Brioude, O. R. Cooper, G. Feingold et al., "of biomass burning on marine stratocumulus clouds off the California coast," *Atmospheric Chemistry and Physics*, vol. 9, no. 22, pp. 8841–8856, 2009.

[65] G. Pandithurai, T. Takamura, J. Yamaguchi et al., "Aerosol effect on cloud droplet size as monitored from surface-based remote sensing over East China Sea region," *Geophysical Research Letters*, vol. 36, no. 13, p. L13805, 2009.

[66] D. Painemal and P. Zuidema, "The first aerosol indirect effect quantified through airborne remote sensing during VOCALS-Rex," *Atmospheric Chemistry and Physics*, vol. 13, no. 2, pp. 917–931, 2013.

[67] M. K. Sporre, E. Swietlicki, P. Glantz, and M. Kulmala, "Aerosol indirect effects on continental low-level clouds over Sweden and Finland," *Atmospheric Chemistry and Physics*, vol. 14, no. 22, pp. 12167–12179, 2014.

[68] G. Harikishan, B. Padmakumari, R. S. Maheskumar, G. Pandithurai, and Q. L. Min, "Aerosol indirect effects from ground-based retrievals over the rain shadow region in Indian subcontinent," *Journal of Geophysical Research: Atmospheres*, vol. 121, 2016.

[69] A. McComiskey, G. Feingold, A. S. Frisch et al., "An assessment of aerosol-cloud interactions in marine stratus clouds based on surface remote sensing," *Journal of Geophysical Research*, vol. 114, no. D9, p. D09203, 2009.

[70] H. Lihavainen, V.-M. Kerminen, and L. A. Remer, "Aerosol-cloud interaction determined by both in situ and satellite data over a northern high-latitude site," *Atmospheric Chemistry and Physics*, vol. 10, no. 22, pp. 10987–10995, 2010.

[71] C. Zhao, S. A. Klein, S. Xie, X. Liu, J. S. Boyle, and Y. Zhang, "Aerosol first indirect effects on non-precipitating low-level liquid cloud properties as simulated by CAM5 at ARM sites," *Geophysical Research Letters*, vol. 39L08806 pages, 2012.

[72] A. Johnson and G. Feingold, "Quantifying error in the radiative forcing of the first aerosol indirect effect," *Geophysical Research Letters*, vol. 35, no. 2, p. L02810, 2008.

[73] F.-M. Breon, "Aerosol effect on cloud droplet size monitored from satellite," *Science*, vol. 295, no. 5556, pp. 834–838, 2002.
[74] W. L. Chameides, C. Luo, R. Saylor et al., "Correlation between model-calculated anthropogenic aerosols and satellite-derived cloud optical depths: indication of indirect effect?" *Journal of Geophysical Research: Atmospheres*, vol. 107, no. D10, 2002.
[75] T. J. Garrett, C. Zhao, X. Dong, G. G. Mace, and P. V. Hobbs, "Effects of varying aerosol regimes on low-level Arctic stratus," *Geophysical Research Letters*, vol. 31, no. 17, pp. a–n, 2004.
[76] I. Gultepe, W. R. Leaitch, C. M. Banic, and G. A. Isaac, "Parameterizations of marine stratus microphysics based on in situ observations: implications for GCMS," *Journal of Climate*, vol. 9, no. 2, pp. 345–357, 1996.
[77] B.-G. Kim, M. A. Miller, S. E. Schwartz, Y. Liu, and Q. Min, "The role of adiabaticity in the aerosol first indirect effect," *Journal of Geophysical Research: Atmospheres*, vol. 113, no. D5, 2008.
[78] G. M. Martin, D. W. Johnson, and A. Spice, "The measurement and parameterization of effective radius of droplets in warm stratocumulus clouds," *Journal of the Atmospheric Sciences*, vol. 51, no. 13, pp. 1823–1842, 1994.
[79] G. M. McFarquhar and A. J. Heymsfield, "Parameterizations of INDOEX microphysical measurements and calculations of cloud susceptibility: applications for climate studies," *Journal of Geophysical Research: Atmospheres*, vol. 106, no. 28, pp. 675–698, 2001.
[80] T. Nakajima, A. Higurashi, K. Kawamoto, and J. E. Penner, "A possible correlation between satellite-derived cloud and aerosol microphysical parameters," *Geophysical Research Letters*, vol. 28, no. 7, pp. 1171–1174, 2001.
[81] J. Quaas, O. Boucher, and F.-M. Bréon, "Aerosol indirect effects in POLDER satellite data and the Laboratoire de Météorologie Dynamique-Zoom (LMDZ) general circulation model," *Journal of Geophysical Research*, vol. 109, no. D8, p. D08205, 2004.
[82] C. H. Twohy, M. D. Petters, J. R. Snider et al., "Evaluation of the aerosol indirect effect in marine stratocumulus clouds: droplet number, size, liquid water path, and radiative impact," *Journal of Geophysical Research*, vol. 110, no. D8, p. D08203, 2005.
[83] K. S. Carslaw, L. A. Lee, C. L. Reddington et al., "contribution of natural aerosols to uncertainty in indirect forcing," *Nature*, vol. 503, no. 7474, pp. 67–71, 2013.
[84] Y. J. Kaufman, I. Koren, L. A. Remer, D. Rosenfeld, and Y. Rudich, "The effect of smoke, dust, and pollution aerosol on shallow cloud development over the Atlantic Ocean," *Proceedings of the National Academy of Sciences*, vol. 102, no. 32, pp. 11207–11212, 2005.
[85] I. Koren, G. Feingold, and L. A. Remer, "The invigoration of deep convective clouds over the Atlantic: aerosol effect, meteorology or retrieval artifact?" *Atmospheric Chemistry and Physics*, vol. 10, no. 18, pp. 8855–8872, 2010.
[86] T. Yuan, Z. Li, R. Zhang, and J. Fan, "Increase of cloud droplet size with aerosol optical depth: an observation and modeling study," *Journal of Geophysical Research*, vol. 113, no. D4, p. D04201, 2008.
[87] T. Nakajima and M. D. King, "Determination of the optical thickness and effective particle radius of clouds from reflected solar radiation measurements. Part I: theory," *Journal of the Atmospheric Sciences*, vol. 47, no. 15, pp. 1878–1893, 1990.
[88] B. Vant-Hull, A. Marshak, L. A. Remer, and Z. Li, "The effects of scattering angle and cumulus cloud geometry on satellite retrievals of cloud droplet effective radius," *IEEE Transactions on Geoscience and Remote Sensing*, vol. 45, no. 4, pp. 1039–1045, 2007.
[89] L. A. Remer et al., "The MODIS aerosol algorithm, products and validation," *Journal of the Atmospheric Sciences*, vol. l62, no. –973, p. 947, 2005.
[90] Z. Li and L. Garand, "Estimation of surface albedo from space: a parameterization for global application," *Journal of Geophysical Research*, vol. 99, no. D4, pp. 8335–8350, 1994.
[91] T. Goren and D. Rosenfeld, "Decomposing aerosol cloud radiative effects into cloud cover, liquid water path and Twomey components in marine stratocumulus," *Atmospheric Research*, vol. 138, pp. 378–393, 2014.